Studies of Inviscid Flux Schemes for Acoustics and Turbulence Problems

C. I. Morris*

NASA Marshall Space Flight Center, Huntsville, AL, 35812, USA

Submitted to the 51st AIAA Aerospace Sciences Meeting, January 7–10, 2013, Grapevine, TX

The last two decades have witnessed tremendous growth in computational power, the development of computational fluid dynamics (CFD) codes which scale well over thousands of processors, and the refinement of unstructured grid-generation tools which facilitate rapid surface and volume gridding of complex geometries. Thus, engineering calculations of $10^7 - 10^8$ finite-volume cells have become routine for some types of problems. Although the Reynolds Averaged Navier Stokes (RANS) approach to modeling turbulence is still in extensive and wide use, increasingly large-eddy simulation (LES) and hybrid RANS-LES approaches are being applied to resolve the largest scales of turbulence in many engineering problems. However, it has also become evident that LES places different requirements on the numerical approaches for both the spatial and temporal discretization of the Navier Stokes equations than does RANS. In particular, LES requires high time accuracy and minimal intrinsic numerical dispersion and dissipation over a wide spectral range. In this paper, the performance of both central-difference and upwind-biased spatial discretizations is examined for a one-dimensional acoustic standing wave problem, the Taylor-Green vortex problem, and the turbulent channel flow problem.

Nomenclature

a	sound speed
E	specific total energy, $e + E_k$
E_k	kinetic energy, $U^2/2$
e	specific internal energy
$\mathbf{f}$	body force per unit volume vector
h	channel half-height, reference length for channel flow problem
k	wavenumber
l	reference length for Taylor-Green vortex problem
M	Mach number, U/a
$\dot{m}$	mass flow rate
N	Number of grid points in a particular direction
p	pressure
Q	Q-criterion, $(\mathbf{R} : \mathbf{R} - \mathbf{S} : \mathbf{S})/2$
$\mathbf{q}$	heat flux
R	gas constant
$\mathbf{R}$	rotation-rate tensor, $(\nabla\mathbf{u} - \nabla\mathbf{u}^T)/2$
$\mathbf{S}$	strain-rate tensor, $(\nabla\mathbf{u} + \nabla\mathbf{u}^T)/2$
T	temperature
t	time
U	velocity magnitude, $\|\mathbf{u}\|$
$\mathbf{u}$	velocity vector

*Aerospace Engineer, Fluid Dynamics Branch/ER42, Senior Member AIAA.

V volume
u, v, w components of velocity vector in the x-, y-, and z-direction, respectively
x, y, z cartesian coordinates

Subscripts

0 denotes an initial condition
c denotes a flow property at the centerline
i, j, k computational indices in the x-, y-, and z-direction, respectively
m denotes a mean flow property
w denotes a flow property at the wall

Symbols

δ kronecker delta
γ ratio of specific heats
λ thermal conductivity
μ viscosity
Ω enstrophy, $\omega \cdot \omega/2$
ω vorticity vector
ϕ generic flowfield quantity
ρ density
τ viscous stress tensor
ε turbulent kinetic energy dissipation rate

Superscripts

$*$ variable normalized by a characteristic flow timescale
$+$ variable normalized by inner-law variables

I. Introduction

Turbulence is a critical factor in most aero- and propulsion-related flows. For many years, the industry-standard approach to incorporating the effect of turbulence in computational fluid dynamics (CFD) calculations has been the Reynolds Averaged Navier Stokes (RANS) modeling approach. RANS implicitly time-averages turbulent motion, and models its effect on the mixing of species, momentum and energy in a flow field. The approach is economical and often allows a CFD calculation to proceed to steady-state. However, it makes several simplifying assumptions, and the results will only be as good as the RANS turbulence model. Meanwhile, the last two decades have witnessed rapid and explosive growth in computational power, the development of CFD codes which scale well over thousands of processors, and the refinement of unstructured grid-generation tools which facilitate rapid surface and volume gridding of complex geometries. CFD engineering calculations of 10^7 – 10^8 finite-volume cells have become routine. Thus, large eddy simulation (LES), which attempts to directly resolve the unsteady motion of the largest scales of turbulence, is increasingly of interest for many fluids engineering problems.[1–3] Additionally, hybrid RANS-LES approaches such as Spalart's Detached Eddy Simulation (DES),[4] which attempt to marry the best strengths of both methods, are in active use.

Because it seeks to accurately resolve the unsteady motion of the largest scales of turbulence, LES places certain requirements on the numerical method used to discretize and advance the Navier Stokes equations. In particular, LES requires high time accuracy and minimal intrinsic numerical dispersion and dissipation over a wide range of length scales. A number of studies in the literature[5–10] have investigated the suitability of various upwind-based shock-capturing schemes for LES. The purpose of this paper is to evaluate the suitability of several different central difference and upwind-biased schemes for a simple one-dimensional acoustic standing wave problem, as well as DNS and LES of the Taylor-Green vortex problem and a turbulent channel flow problem.

II. Governing Equations

The compressible Navier-Stokes equations for a single chemical species are the governing model for this study. The time-dependent differential form of these equations is written as follows:

$$\frac{\partial \rho}{\partial t} + \nabla \cdot (\rho \mathbf{u}) = 0 \tag{1}$$

$$\frac{\partial \rho \mathbf{u}}{\partial t} + \nabla \cdot (\rho \mathbf{u}\mathbf{u} + p\delta) = \nabla \cdot \tau + \mathbf{f} \tag{2}$$

$$\frac{\partial \rho E}{\partial t} + \nabla \cdot (\rho \mathbf{u}(E + p)) = \nabla \cdot (\mathbf{u} \cdot \tau - \mathbf{q}) + \mathbf{f} \cdot \mathbf{u} \tag{3}$$

A calorically perfect ideal gas equation of state is used: $p = \rho RT$, and $T = (\gamma - 1)e/R$. $\gamma = 1.4$ and $R = 287\,\mathrm{J/Kg\text{-}K}$ for all cases studied in this work. The viscous stress tensor, τ is defined as

$$\tau = 2\mu \mathbf{S} - \frac{2}{3}\mu(\nabla \cdot \mathbf{u})\delta \tag{4}$$

and the heat flux vector as

$$\mathbf{q} = -\lambda \nabla T \tag{5}$$

The transport properties μ and λ are calculated using the Sutherland formulas for air.

III. Numerical Method

The Navier-Stokes equations are solved by the finite-difference method in the conventional cartesian coordinate system. The inviscid flux (the second term on the left-hand side of Eqs. 1, 2, and 3) is the portion of the equations that deals with convection of mass, momentum and energy. Historically, the discretization of these terms has been a driving issue in CFD research since its inception. Four central difference (CD) schemes, four upwind-biased (UB) schemes, and the Fromm scheme for the inviscid flux are evaluated in this work. The stencil coefficients for these schemes are shown in table 1 for a generic flowfield quantity, ϕ. The number in the name for each scheme denotes the formal order of accuracy. Conservative differencing was used such that, at node i,j,k, the derivative in the x-direction is given by:

$$\frac{\partial \phi_{i,j,k}}{\partial x} = \frac{\phi_{i+1/2,j,k} - \phi_{i-1/2,j,k}}{\Delta x} \tag{6}$$

where $\phi_{i+1/2,j,k}$ and $\phi_{i-1/2,j,k}$ are interpolated and formed in such a way that the final difference is equivalent to one of the stencils shown in Table 1. For example, $\phi_{i+1/2,j,k} = (\phi_{i,j,k} + \phi_{i+1,j,k})/2$ and $\phi_{i-1/2,j,k} = (\phi_{i-1,j,k} + \phi_{i,j,k})/2$ yields the CD-2 formula, while $\phi_{i+1/2,j,k} = (-\phi_{i-1,j,k} + 5\phi_{i,j,k} + 2\phi_{i+1,j,k})/6$ and $\phi_{i-1/2,j,k} = (-\phi_{i-2,j,k} + 5\phi_{i-1,j,k} + 2\phi_{i,j,k})/6$ yields the UB-3 formula. It should be noted that the UB and Fromm schemes shown assume convection in the positive-x direction. A reflected stencil (about $\phi_{i,j,k}$) would be employed for convection in the negative-x direction.

Note that the inviscid flux terms contain combinations of several different primitive flow variables. For example, in the x-direction, the terms to be differenced are $\phi = [\rho u, \rho u^2 + p, \rho uv, \rho uw, \rho u(E + p)]^T$. In divergence form central differencing, the flux values themselves are directly differenced. In skew-symmetric form central differencing, the flux is formed from a combination of central differences of the flux values and the component flow property variables themselves. The central difference schemes investigated here employ the skew-symmetric approach. This approach has been investigated by several researchers in recent years,[11–16] and appears to be more accurate and stable than divergence form central differencing. In particular, the implementation of Ref. 15 for the skew-symmetric scheme of Ref. 13 was used. Additional detail will be provided in the final paper.

Upwinding can be implemented by various methods in a CFD code.[17,18] In this work, first a leftward-biased interpolation for the primitive flow variables $\phi = \rho$, u, v, w, and p at the half-node is formed which is consistent with the UB and Fromm formulas from Table 1. The remaining state variables are calculated using the perfect gas law, and the inviscid flux terms are then calculated from these components. The process is then repeated for a rightward-biased interpolation for a half-node using a reflected stencil. The final value

Table 1. Coefficients for central difference and upwind-biased stencils for $\partial\phi_{i,j,k}/\partial x = (\phi_{i+1/2,j,k} - \phi_{i-1/2,j,k})/\Delta x$. The upwind-biased (UB) and Fromm stencils assume convection in the positive-x direction.

Name	ϕ_{i-4}	ϕ_{i-3}	ϕ_{i-2}	ϕ_{i-1}	ϕ_i	ϕ_{i+1}	ϕ_{i+2}	ϕ_{i+3}	ϕ_{i+4}
CD-2				-1/2		1/2			
CD-4			1/12	-2/3		2/3	-1/12		
CD-6		-1/60	3/20	-3/4		3/4	-3/20	1/60	
CD-8	1/280	-4/105	1/5	-4/5		4/5	-1/5	4/105	-1/280
UB-1				-1	1				
UB-3			1/6	-1	1/2	1/3			
UB-5		-1/30	1/4	-1	1/3	1/2	-1/20		
UB-7	1/140	-7/105	3/10	-1	1/4	3/5	-1/10	1/105	
Fromm-2			1/4	-5/4	3/4	1/4			

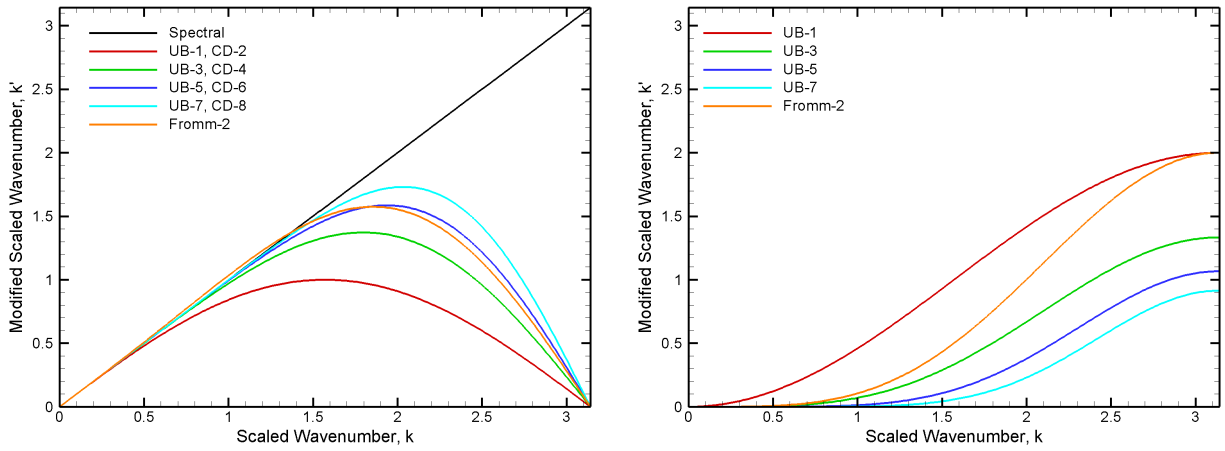

(a) Dispersion Error

(b) Dissipation Error

Figure 1. Fourier analysis of spatial discretization schemes studied in this work.

of the inviscid flux at the half-node is provided by the Roe approximate Riemann solver,[19] using these two separate left and right states. Again, additional detail on the method will be provided in the final paper.

Plots of the dispersion error and dissipation error from a fourier analysis of the various schemes are shown in figure 1. The scaled wavenumber is equal to $2\pi k/N$, such that it is equal to π at the spatial Nyquist frequency. As discussed by Li,[20] the dispersion error of each of the UB schemes is equal to that of the CD scheme of the next higher order of accuracy. All of the CD schemes are free of dissipation error, while the UB and Fromm schemes experience an increasing dissipation error at higher wavenumbers. The higher-order UB schemes have a significantly smaller dissipation error than the lower-order ones.

The viscous terms were discretized using 2$^{\text{nd}}$ order central differences. All schemes were advanced using a low-storage 4-stage, 2$^{\text{nd}}$ order accurate Runge-Kutta time advancement algorithm.

IV. Results and Discussion

IV.A. One-Dimensional Acoustic Standing Wave Problem

As a simple means of evaluating the ability of the various inviscid flux schemes to resolve high-frequency acoustics or flowfield variations, they were tested on a one-dimensional acoustic standing wave problem. This problem assumes a one-dimensional computational domain with periodic boundary conditions. 128 grid points are used. The domain is initialized with air at $p = 0.25\,\text{atm}$, $T = 298.15\,\text{K}$, and a small sinusoidal velocity variation as a function of axial distance, x, and specified wavenumber, k: $u(x, t = 0) = (0.1\,\text{m/s})\cos(kx)$. Under the assumption of isentropic, small disturbance inviscid flow, the Navier-Stokes equations can be simplified to the linearized equations of gas dynamics, and an exact solution derived: $u(x,t) = (0.05\,\text{m/s})(\cos(k(x-at)) + \cos(k(x+at))) = (0.1\,\text{m/s})\cos(kx)\cos(kat)$, where t is time and a is the sound speed (346.117 m/s). Due to space limitations in this abstract, the results from this analysis cannot be shown. However, in summary, the results clearly demonstrate the fourier characteristics shown in figure 1. The exact solution can even be modified to account for the dispersion and dissipation error of a particular scheme, and the resulting equation has excellent agreement with the numerical results. The complete results from this analysis will be presented in the final paper.

IV.B. Taylor-Green Vortex Problem

The Taylor-Green vortex problem is a benchmark case which, from a smooth initial condition, simulates vortex stretching and transition to turbulence. It was used as a test case for the 1st International Workshop on High-Order CFD Methods, held at the 50th AIAA Aerospace Sciences Meeting, January 7–8, 2012, in Nashville, Tennessee. DNS results have been calculated by Brachet et al.[21] and, more recently by van Rees et al.[22] The latter results are used as the basis for comparison in this paper.

The solution is computed on a periodic cube domain, $-\pi l \leq x, y, z \leq \pi l$. The flowfield is initialized with:

$$\begin{aligned} u &= U_0 \sin\left(\frac{x}{l}\right)\cos\left(\frac{y}{l}\right)\cos\left(\frac{z}{l}\right), \\ v &= -U_0 \cos\left(\frac{x}{l}\right)\sin\left(\frac{y}{l}\right)\cos\left(\frac{z}{l}\right), \\ w &= 0, \\ p &= p_0 + \frac{\rho_0 U_0^2}{16}\left[\cos\left(\frac{2x}{l}\right) + \cos\left(\frac{2y}{l}\right)\right]\left[\cos\left(\frac{2z}{l}\right) + 2\right] \end{aligned} \tag{7}$$

where here $l = 0.01\,\text{m}$, $p_0 = 7271\,\text{Pa}$, $T_0 = 298.15\,\text{K}$ and $U_0 = 34.612\,\text{m/s}$. The flow is effectively incompressible, $M_0 = U_0/a_0 = 0.1$. The initial condition for ρ is calculated by the perfect gas law, assuming fixed $T = T_0$. The transport properties are fixed at their values at T_0 throughout the calculation. The resultant Reynolds number is $Re = \rho_0 U_0 l/\mu_0 = 1600$.

The time evolution of the Taylor-Green vortex flowfield can be visualized by showing iso-surfaces of zero Q-criterion ($Q = 0$) at various times (figure 2). $Q > 0$ indicates regions of a flowfield in which vorticity dominates over strain. This calculation was performed using the CD-4 scheme on a 192^3 point grid, with uniform grid spacing throughout the domain. Time is normalized by a characteristic timescale, $t^* = tU_0/l$, and the iso-surfaces are colored with the normalized velocity magnitude, U/U_0. It is evident from the figure that the initial large-scale ($k = 1$) vortex structure at $t^* = 0$ steadily evolves toward smaller vortex structures ($t^* = 4$). By $t^* = 8$, the flow has transitioned to turbulence, and proceeds steadily to a more isotropic state. The symmetries in the flowfield, discussed by Ref. 21, are evident from figure 2. Also note that the reduction in overall kinetic energy as the simulation progresses is visible in the velocity color scale .

Time histories for the mean kinetic energy, kinetic energy dissipation rate, and enstrophy for the CD-4 and UB-3 schemes on a 192^3 point grid are compared with the spectral DNS (on a 512^3 point grid) of Ref. 22 in figures 3, 4, and 5, respectively. The mean kinetic energy for the domain is given by

$$E_{k,m} = \frac{1}{\rho_0 V}\int \rho \frac{U^2}{2} dV \tag{8}$$

and the mean kinetic energy dissipation rate is $\varepsilon = -\partial E_{k,m}/\partial t$. The mean enstrophy for the domain is given

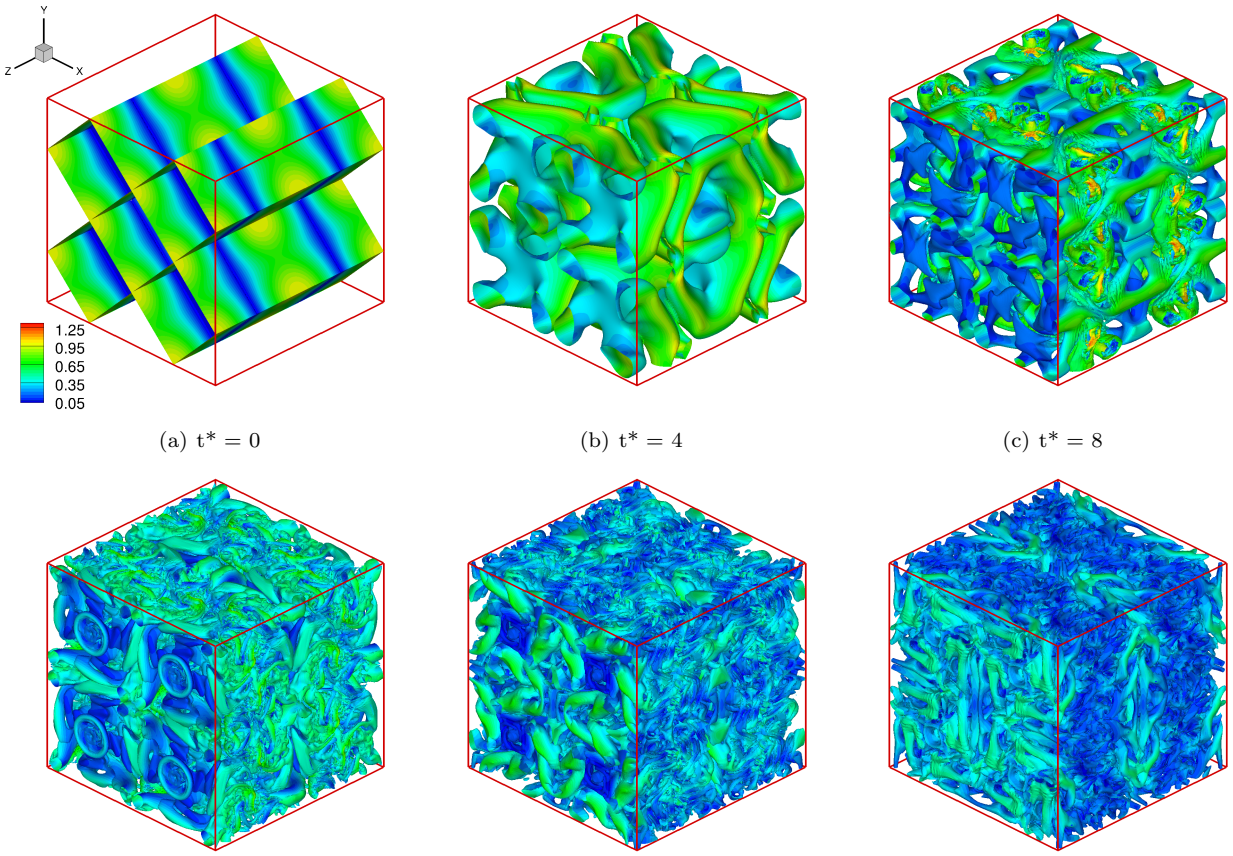

(a) t* = 0 (b) t* = 4 (c) t* = 8

(d) t* = 12 (e) t* = 16 (f) t* = 20

Figure 2. Iso-surfaces of zero Q-criterion showing the time evolution of the Taylor-Green vortex problem at $Re = 1600$, computed with the CD-4 scheme on a 192^3 grid. Iso-surfaces are colored with the normalized velocity magnitude, U/U_0. t* is a normalized timescale, tU_0/l

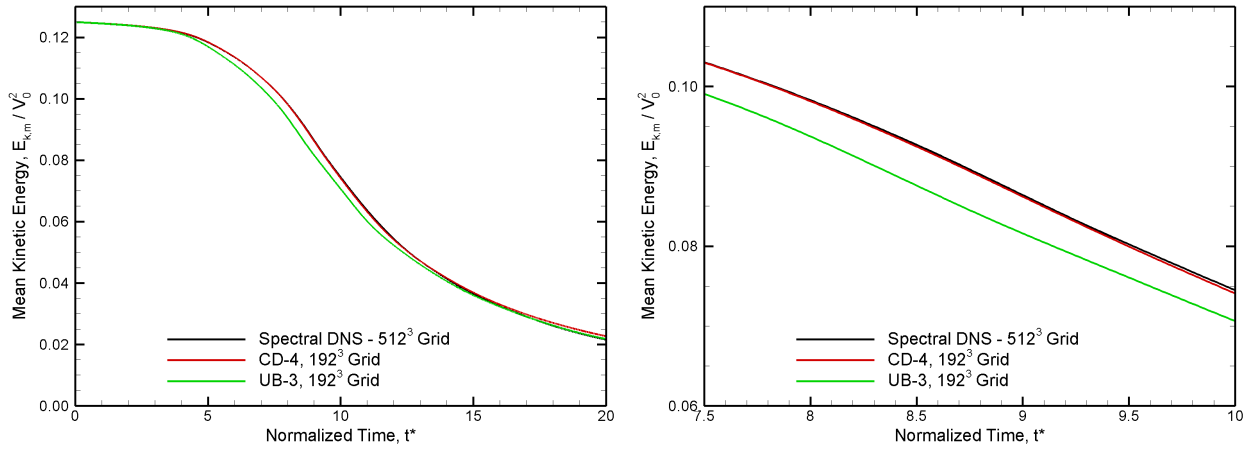

(a) Overview (b) Closeup of $t^* = 7.5$ to $t^* = 10$

Figure 3. Plots showing the time evolution of the normalized mean kinetic energy, $E_{k,m}/V_0^2$ for the reference spectral DNS on a 512^3 point grid, and the CD-4 and UB-3 schemes on 192^3 point grids.

by

$$\Omega_m = \frac{1}{\rho_0 V} \int \rho \frac{\omega \cdot \omega}{2} dV \tag{9}$$

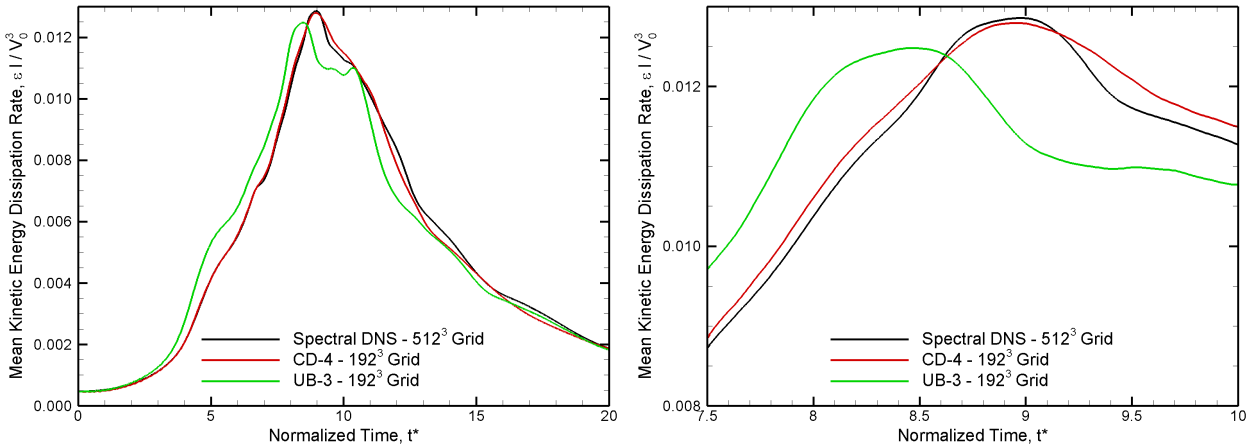

(a) Overview (b) Closeup of $t^* = 7.5$ to $t^* = 10$

Figure 4. Plots showing the time evolution of the normalized mean kinetic energy dissipation rate, $\varepsilon l/V_0^3$ for the reference spectral DNS on a 512^3 point grid, and the CD-4 and UB-3 schemes on 192^3 point grids.

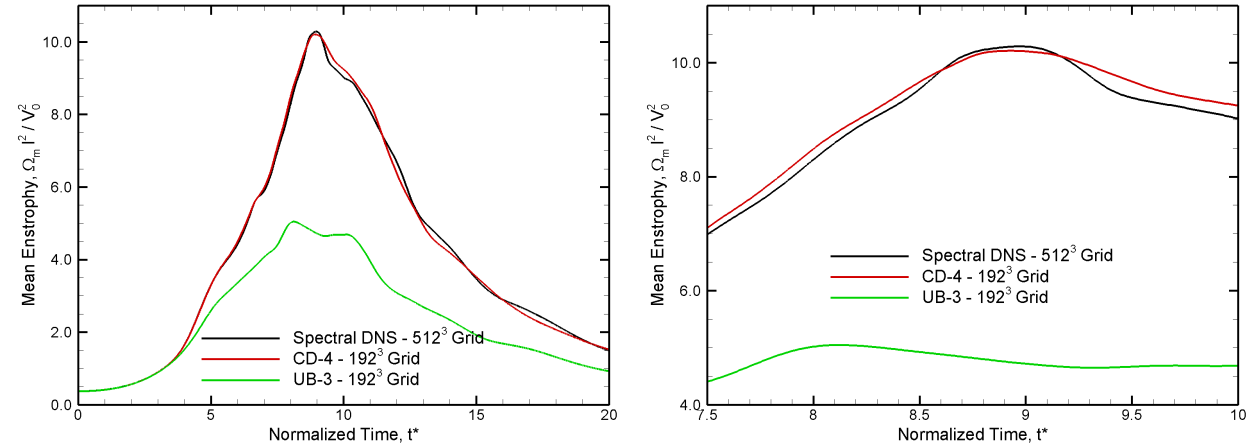

(a) Overview (b) Closeup of $t^* = 7.5$ to $t^* = 10$

Figure 5. Plots showing the normalized mean enstrophy, $\Omega l^2/V_0^2$ for the reference spectral DNS on a 512^3 point grid, and the CD-4 and UB-3 schemes on 192^3 point grids.

It is evident from figures 3, 4, and 5 that the CD-4 scheme at this grid resolution is in very good agreement with the reference DNS results for all three mean flow properties. The UB-3 scheme follows the mean kinetic energy history reasonably well, although it consistently dissipates the kinetic energy faster than the DNS through $t^* = 8.6$. The mean enstrophy history for the UB-3 scheme begins to diverge below the DNS at $t^* = 3.5$, and remains significantly smaller throughout the remainder of the simulation. This is likely due to the dissipative nature of the UB-3 scheme at higher wavenumbers, which become more and more significant as the simulation progresses.

Thus far, simulations for all schemes have been completed on a 128^3 point grid, the CD-4, CD-6 and UB-3 schemes on a 192^3 point grid, and the CD-6 scheme on a 256^3 point grid. In the final paper, the schemes will be compared on grids ranging from 64^3 – 256^3 points to assess the suitability of the schemes for both DNS and LES of the Taylor-Green vortex.

IV.C. Turbulent Channel Flow Problem

Turbulent channel flow has been extensively studied by experiments[23] and DNS studies,[24,25] and the mean flow profile and statistics have been very well characterized. Therefore, it is an excellent benchmark case for

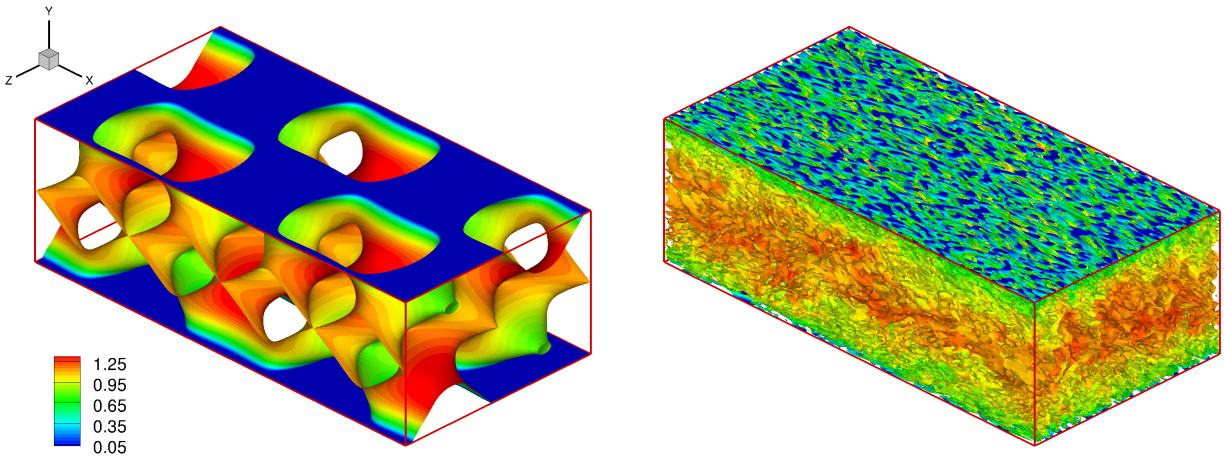

(a) t* = 0 (b) t* = 30

Figure 6. Iso-surfaces of zero Q-criterion showing turbulent channel flow at $Re = 14300$, computed with the CD-2 scheme on a 128 × 129 × 128 point grid. a) initial condition, b) statistically stationary state. Iso-surfaces are colored with the normalized velocity magnitude, U/u_m. t* is a normalized timescale, $t^* t u_m/2\pi h$, representing the number of streamwise flowthrough times.

evaluating various inviscid flux schemes for DNS or LES of wall-bounded shear flows. Here, turbulent channel flow of air at $p = 0.25\,\text{atm}$, $T = 298.15\,\text{K}$ and a mean streamwise velocity $u_m = 44.44\,\text{m/s}$ is simulated. The flow is essentially incompressible ($M_m = 0.127$). The computational domain is $0 \le x \le 2\pi h$ in the streamwise (x-) direction, $-h \le y \le h$ in the vertical (y-) direction, and $0 \le z \le \pi h$ in the spanwise (z-) direction. The channel half-width, h, is 0.01 m. The Reynolds number based on the full channel width, $2h$, is $Re = \rho_m u_m 2h/\mu_m = 14300$.

Periodic boundary conditions are used in both the x- and z-directions. Adiabatic, no-slip wall boundary conditions are imposed on the bottom and top (y-) surfaces. In order to prevent the viscous losses at both walls from slowly "wearing down" the flow, the integrated area-sum of these forces is computed at each time step, and added in as a body force term, f, over the entire computational volume. This term effectively reproduces the effect of the pressure gradient needed to sustain a real turbulent channel flow, and maintains a constant mass flow rate in the simulation.

The flow is initialized using a power law mean velocity profile, along with unit wavenumber ($k = 1$) oscillations in y and z, and $k = 2$ wavenumber oscillations in x. This divergence-free initial condition was borrowed from Moin and Kim.[26]

$$\begin{aligned} u &= u_{c,0}\left[1-\left(\frac{y}{h}\right)^8\right] + U_0\pi\cos\left(\frac{2x}{h}\right)\sin\left(\frac{\pi y}{h}\right)\sin\left(\frac{2z}{h}\right), \\ v &= -U_0\sin\left(\frac{2x}{h}\right)\left[1+\cos\left(\frac{\pi y}{h}\right)\right]\sin\left(\frac{2z}{h}\right), \\ w &= -U_0\frac{\pi}{2}\sin\left(\frac{2x}{h}\right)\sin\left(\frac{\pi y}{h}\right)\cos\left(\frac{2z}{h}\right) \end{aligned} \tag{10}$$

where here the initial centerline streamwise velocity, $u_{c,0} = 50\,\text{m/s}$ and $U_0 = 5\,\text{m/s}$.

This initial condition, as well as a fully developed turbulent channel flow, can be visualized by showing iso-surfaces of zero Q-criterion ($Q = 0$) at $t^* = 0$ and $t* = 30$ (figure 6). t* is a normalized timescale, $t^* = tu_m/2\pi h$, representing the number of streamwise flowthrough times. The iso-surfaces are colored with the normalized velocity magnitude, U/u_m. This calculation was performed using the CD-2 scheme on a $128 \times 129 \times 128$ point grid. The grid spacing is uniform in x and z, and stretched by the hyperbolic tangent function in y. The wall-normal grid spacing at the walls is $0.001h$. Grid spacings normalized by the wall friction lengthscale are: $\Delta x^+ = \Delta x\sqrt{(\tau_w\rho_w)}/\mu_w = 20.1$, $\Delta y_w^+ = 0.426$, $\Delta y_c^+ = 16.4$, $\Delta z^+ = 10.0$.

Skin friction coefficient histories for the various inviscid flux schemes are shown in figure 7. The CD schemes were started from the initial condition, and it is evident from the skin friction history that the flow rapidly transitions to turbulence within the first few flowthrough times. The solutions were time-averaged from $t^* = 15$–30, as well as space-averaged in the periodic directions x and z. The time- and space-averaged

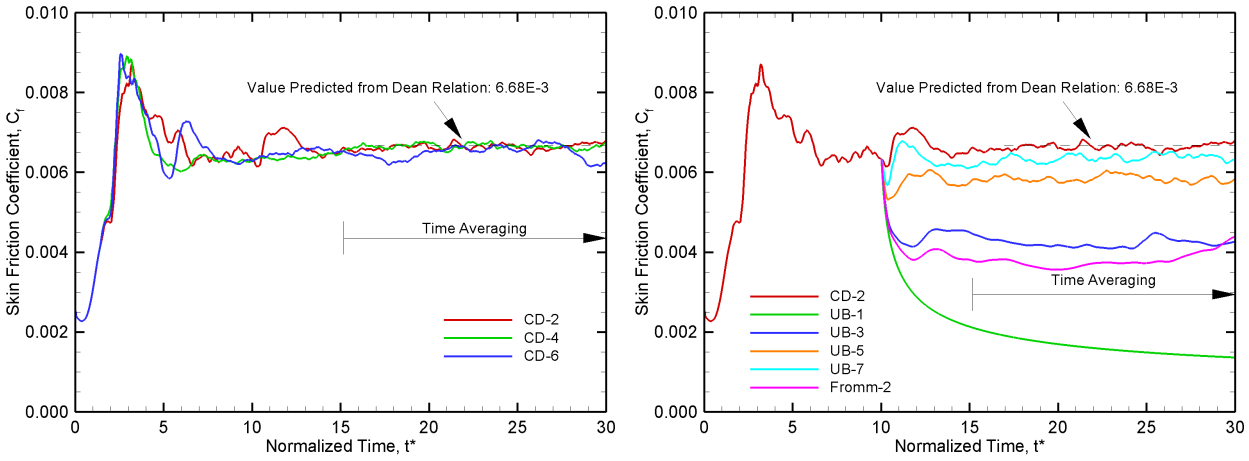

(a) CD-2, CD-4 and CD-6 (b) CD-2, UB-1, UB-3, UB-5, UB-7, and Fromm-2

Figure 7. Comparison of skin friction coefficient history for the inviscid flux schemes on a 128 × 129 × 128 point grid.

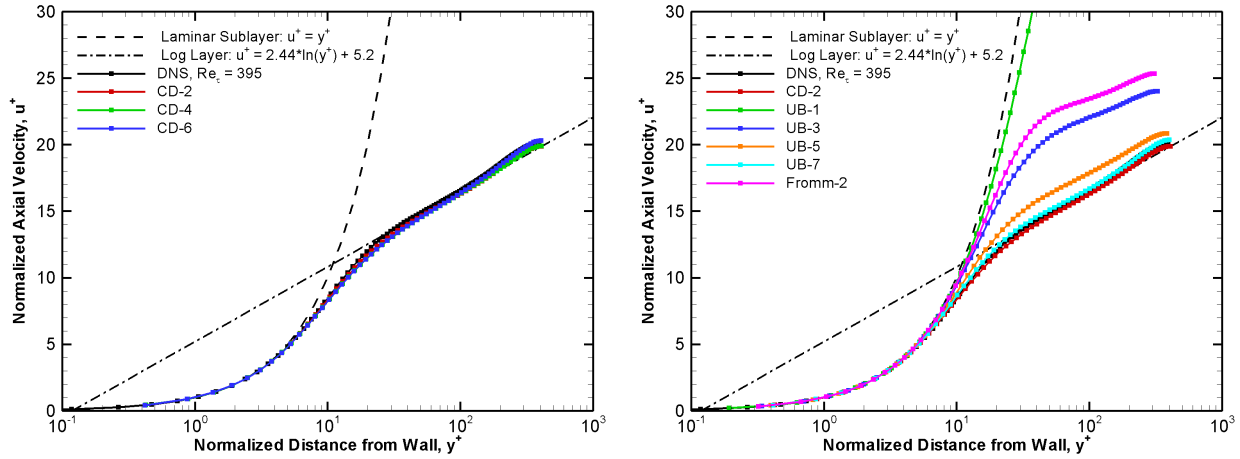

(a) CD-2, CD-4 and CD-6y (b) CD-2, UB-1, UB-3, UB-5, UB-7, and Fromm-2

Figure 8. Comparison of streamwise velocity profiles for the inviscid flux schemes on a 128 × 129 × 128 point grid.

skin friction coefficient for all three CD schemes is in excellent agreement (within 3%) with the predictions from the reference Dean[23] correlation at this Reynolds number. The UB and Fromm schemes were started from the CD-2 solution at $t^* = 10$. As might be expected, the UB-1 scheme rapidly begins to laminarize the flow, but has not achieved a steady state condition even by $t^* = 30$. The UB-3, UB-5 and UB-7 schemes do achieve a stationary state by $t^* = 15$, and their time- and space-averaged coefficient values are in progressively closer agreement with the CD-2 results and the prediction from the Dean correlation. The average skin friction for the Fromm-2 scheme is slightly lower than the UB-3 scheme.

The time- and space-averaged streamwise velocity profiles for the schemes (except UB-1 which is only space-averaged at $t^* = 30$) are compared with the laminar sublayer profile, the log-law profile, and the DNS results of Moser et al.[25] in figure 8. The velocity profiles are normalized by the characteristic wall friction velocity, $u^+ = u/\sqrt{(\tau_w/\rho_w)}$, and the distance from the wall is normalized by the wall friction lengthscale, $y^+ = |y - y_w|\sqrt{(\tau_w \rho_w)}/\mu_w$ The results are consistent with the observations from the skin friction history.

Thus far, simulations for all of schemes have been completed on a 128 × 129 × 128 point grid, the CD-2 scheme on a 192 × 193 × 192 point grid, and the CD-2, CD-4 and CD-6 schemes on progressively coarser 96 × 129 × 96, 64 × 129 × 64, and 48 × 129 × 48 point grids. In the final paper, the suitability of all of the schemes for DNS and LES of turbulent channel flow will be assessed. The effect of the Smagorinsky and Dynamic Smagorinsky subgrid models on the results will also be determined.

References

[1]Moin, P., "Numerical and Physical Issues in Large Eddy Simulation of Turbulent Flows," *JSME International Journal, Series B*, Vol. 41, No. 2, 1998, pp. 454 – 463.

[2]Fureby, C., "Towards the use of large eddy simulation in engineering," *Progress in Aerospace Sciences*, Vol. 44, No. 6, 2008, pp. 381 – 396.

[3]Georgiadis, N. J., Rizzetta, D. P., and Fureby, C., "Large-Eddy Simulation: Current Capabilities, Recommended Practices, and Future Research," *AIAA Journal*, Vol. 48, No. 8, 2010, pp. 1772 – 1784.

[4]Spalart, P. R., Jou, W.-H., Strelets, M., and Allmaras, S. R., "Comments on the feasibility of LES for wings, and on a hybrid RANS/LES approach," In "Advances in DNS/LES: proceedings of the First AFOSR International Conference on DNS/LES", C. Liu and Z. Liu Eds., Greyden Press, Columbus, OH.

[5]Mittal, R. and Moin, P., "Suitability of Upwind-Biased Finite Difference Schemes for Large-Eddy Simulation of Turbulent Flows," *AIAA Journal*, Vol. 35, No. 8, 1997, pp. 1415 – 1417.

[6]Garnier, E., Mossi, M., Sagaut, P., Comte, P., and Deville, M., "On the Use of Shock-Capturing Schemes for Large-Eddy Simulation," *Journal of Computational Physics*, Vol. 153, No. 2, 1999, pp. 273 – 311.

[7]Mossi, M. and Sagaut, P., "Numerical investigation of fully developed channel flow using shock-capturing schemes," *Computers & Fluids*, Vol. 32, No. 2, 2003, pp. 249 – 274.

[8]Larsson, J., Lele, S. K., and Moin, P., "Effect of numerical dissipation on the predicted spectra for compressible turbulence," Technical Report, Annual Research Briefs, Center for Turbulence Research, Stanford University, 2007.

[9]Johnsen, E., Larsson, J., Bhagatwala, A. V., Cabot, W. H., Moin, P., Olson, B. J., Rawat, P. S., Shankar, S. K., Sjögreen, B., Yee, H., Zhong, X., and Lele, S. K., "Assessment of high-resolution methods for numerical simulations of compressible turbulence with shock waves," *Journal of Computational Physics*, Vol. 229, No. 4, 2010, pp. 1213 – 1237.

[10]Pirozzoli, S., "Numerical Methods for High-Speed Flows," *Annual Review of Fluid Mechanics*, Vol. 43, No. 1, 2011, pp. 163 – 194.

[11]Ducros, F., Laporte, F., Soulres, T., Guinot, V., Moinat, P., and Caruelle, B., "High-Order Fluxes for Conservative Skew-Symmetric-like Schemes in Structured Meshes: Application to Compressible Flows," *Journal of Computational Physics*, Vol. 161, No. 1, 2000, pp. 114 – 139.

[12]Honein, A. E. and Moin, P., "Higher entropy conservation and numerical stability of compressible turbulence simulations," *Journal of Computational Physics*, Vol. 201, No. 2, 2004, pp. 531 – 545.

[13]Kennedy, C. A. and Gruber, A., "Reduced aliasing formulations of the convective terms within the NavierStokes equations for a compressible fluid," *Journal of Computational Physics*, Vol. 227, No. 3, 2008, pp. 1676 – 1700.

[14]Subbareddy, P. K. and Candler, G. V., "A fully discrete, kinetic energy consistent finite-volume scheme for compressible flows," *Journal of Computational Physics*, Vol. 228, No. 5, 2009, pp. 1347 – 1364.

[15]Pirozzoli, S., "Generalized conservative approximations of split convective derivative operators," *Journal of Computational Physics*, Vol. 229, No. 19, 2010, pp. 7180 – 7190.

[16]Pirozzoli, S., "Stabilized non-dissipative approximations of Euler equations in generalized curvilinear coordinates," *Journal of Computational Physics*, Vol. 230, No. 8, 2011, pp. 2997 – 3014.

[17]Zhong, X., "High-Order Finite-Difference Schemes for Numerical Simulation of Hypersonic Boundary-Layer Transition," *Journal of Computational Physics*, Vol. 144, No. 2, 1998, pp. 662 – 709.

[18]Rehman, S. F., Eldredge, J. D., Zhong, X., and Kim, J., "A Simple and Robust Approach for Higher Order Hybrid Shock Capturing Methods," AIAA Paper 2010-4453, June 2010.

[19]Roe, P., "Approximate Riemann solvers, parameter vectors, and difference schemes," *Journal of Computational Physics*, Vol. 43, No. 2, 1981, pp. 357 – 372.

[20]Li, Y., "Wavenumber-Extended High-Order Upwind-Biased Finite-Difference Schemes for Convective Scalar Transport," *Journal of Computational Physics*, Vol. 133, No. 2, 1997, pp. 235 – 255.

[21]Brachet, M. E., Meiron, D. I., Orszag, S. A., Nickel, B. G., Morf, R. H., and Frisch, U., "Small-scale structure of the Taylor-Green vortex," *Journal of Fluid Mechanics*, Vol. 130, 1983, pp. 411 – 452.

[22]van Rees, W. M., Leonard, A., Pullin, D., and Koumoutsakos, P., "A comparison of vortex and pseudo-spectral methods for the simulation of periodic vortical flows at high Reynolds numbers," *Journal of Computational Physics*, Vol. 230, No. 8, 2011, pp. 2794 – 2805.

[23]Dean, R. B., "Reynolds Number Dependence of Skin Friction and Other Bulk Flow Variables in Two-Dimensional Rectangular Duct Flow," *Journal of Fluids Engineering*, Vol. 100, No. 2, 1978, pp. 215 – 223.

[24]Kim, J., Moin, P., and Moser, R., "Turbulence statistics in fully developed channel flow at low Reynolds number," *Journal of Fluid Mechanics*, Vol. 177, 1987, pp. 133 – 166.

[25]Moser, R. D., Kim, J., and Mansour, N. N., "Direct numerical simulation of turbulent channel flow up to $\mathrm{Re}_\tau = 590$," *Physics of Fluids*, Vol. 11, No. 4, 1999, pp. 943 – 945.

[26]Moin, P. and Kim, J., "On the numerical solution of time-dependent viscous incompressible fluid flows involving solid boundaries," *Journal of Computational Physics*, Vol. 35, No. 3, 1980, pp. 381 – 392.